JCTC Journal of Chemical Theory and Computation

Article

pubs.acs.org/JCTC

On the Electronic and Geometric Structures of $FeO_2^{-/0}$ and the Assignment of the Anion Photoelectron Spectrum

Marc F. A. Hendrickx* and Van Tan Tran

Afdeling Kwantumchemie en Fysicochemie, Departement Chemie, Katholieke Universiteit Leuven, Celestijnenlaan 200F, B-3001 Heverlee-Leuven, Belgium

ABSTRACT: The photoelectron spectrum of FeO_2^- has been assigned by performing geometry optimizations at the CASPT2 and RCCSD(T) levels of computation. All relevant states are found to possess floppy C_{2v} geometrical structures as the Renner-Teller splittings of the linear states are extremely small and the corresponding energy barriers for the OFeO bond angle inversions are calculated in the range of a few hundred wavenumbers. In this sense, the description of the electronic structure in terms of the $D_{\infty h}$ point group is acceptable, and the experimentally proposed linear structure for FeO_2^- is theoretically confirmed. High accuracy single-point multireference RASPT2 and single-reference RCCSD(T) calculations support a $^2\Delta_g$ as the ground state of the anion, even though the energy differences between the $^4\Pi_g$ and $^6\Sigma_g^+$ states are smaller than 0.2 eV. After this identification of the doublet ground state, the photoelectron spectra of FeO_2^- could be assigned in all aspects. The $^2\Delta_g \rightarrow {}^3\Delta_g$ ionization appears to be at the origin of the X band at 2.36 eV, while the A band at 3.31 eV should be ascribed to the $^2\Delta_g \rightarrow {}^3\Sigma_g^+$ ionization. This assignment is substantiated by Franck−Condon factors for which BP86 optimized geometries and harmonic vibrational frequencies were employed. Indeed, no pronounced vibrational progression should be observed since both bands involve electron detachments out of nonbonding mainly 3d iron molecular orbitals.

INTRODUCTION

Compounds possessing iron−oxygen bonds are of key importance to a vast amount of industrial and biological chemical processes.[1−5] In this context, a large body of experimental work and quantum chemical studies has been published for some small elementary iron−oxygen clusters.[6] In particular, the reaction products of iron atoms with molecular dioxygen in condensing argon have been studied with matrix infrared and Mössbauer spectroscopy.[7−11] Detailed photoelectron spectra of mono- and diiron oxide molecules (FeO_n^- and $Fe_2O_n^-$ (n = 1−4)) are available and provide an important guidance for the description of their gas phase geometric structures and electronic properties.[12−15] However, the available experimental data such as electron affinities, different ionization energies, and vibrational frequencies are not sufficient to derive a conclusive assignment for the observed bands to a specific isomer or for a comprehensive description of its electronic structure. As a first exploration of the potential energy surfaces for the different mass spectrometric observed stoichiometries $FeO_n^{-/0}$, various density functional theory (DFT) methods have been widely employed for obtaining an elementary idea about the relative stabilities of the various isomers as they are possibly formed by laser ablation in plasma by unknown clusterification processes.[8,16−21] However, due to the large number of closely spaced low-lying electronic states of these iron-oxide clusters, and the expected multireference character of their electronic structure, wave function methods such as complete or restricted active space second-order perturbation theory (CASPT2, RASPT2), multireference configuration interaction (MRCI), and restricted coupled cluster (RCCSD(T)) have since been proven to be of crucial importance for obtaining a more in-depth analysis into their structural and electronic properties.[22−27]

Among the monoiron oxides, the computational determination of the ground states of FeO_2 and its anion appears to be an extremely difficult matter. The small energy differences between various low-lying states and the shallow potential energy curves in the vicinity of their equilibrium geometries cause different computational methods to predict different types of ground states and relative positions of the low-lying excited states. This makes the assignment of the experimental anion photoelectron spectra a particularly challenging task, moreover because the neutral cluster has a large number of excited states that must be considered as being responsible for the observed bands. Three different types of isomers of the $FeO_2^{-/0}$ stoichiometry were previously considered in the context of matrix-isolation Mössbauer[7] or infrared spectroscopy[7,8,11] and subsequently studied with various kinds of DFT methods.[9,11,16−18,23,28−31] All studies agree that the most stable isomer for the neutral and anionic clusters is either a bent C_{2v} or a closely related linear $D_{\infty h}$ dioxide structure, which both possess two equivalent iron−oxygen bonds with no direct O−O bond. Because of the small energy differences between the lowest states of FeO_2^-, DFT calculations can only tentatively predict the $^4B_2$ state of the bent C_{2v} structure as the ground state. The calculated energy gaps between the lowest sextet or doublet states are in some circumstances smaller than a tenth of an eV. Also the prediction of the ground state of the neutral FeO_2 cluster depends on the choice of the functional. Due to the bias of the hybrid B3LYP method for high-spin states, the ionization from $^4B_2$ to $^3B_1$ was found, as a single-electron detachment, to correspond to the lowest binding energy X band in the anion photoelectron spectrum.[18,31] These attempts

Received: May 2, 2012
Published: August 15, 2012

   dx.doi.org/10.1021/ct300516y | J. Chem. Theory Comput. 2012, 8, 3089−3096

to assign the anion photoelectron spectrum are at present unsatisfactory because a recent combined matrix isolation infrared spectroscopic and quantum chemical computational study supported the $^2\Delta_g$ state with a linear $D_{\infty h}$ structure instead of the bent $^4B_2$ (C_{2v}) state as the ground state of the anion.[23] By comparing a large body of computational methods it was advocated by the authors that the use of a multireference computational technique is of absolute necessity to reach this conclusion. In the light of this recent result, the previously made assignment of the photoelectron spectrum of FeO_2^- needs to be reinvestigated at a comparable wave function level of theory. As an additional motivation of our detailed analysis of the photoelectron spectroscopy of FeO_2^-, an even more recent computational study ascribed the adiabatic electron affinity of FeO_2 as the energy difference between the $^3B_1$ state of the neutral cluster and the $^4B_1$ ground state of FeO_2^-.

In the present contribution, a large number of theoretical methods ranging from DFT and single-reference RCCSD(T) (restricted coupled-cluster with single and double and perturbative triple excitations) to the multireference CASPT2 and RASPT2 methods will be applied to the $FeO_2^{-/0}$ clusters. By utilizing the RCCSD(T) and RASPT2 methods, as high accuracy wave function techniques, we will attempt to identify which state of the FeO_2^- cluster is responsible for its photoelectron spectrum and for the adiabatic electron affinity of FeO_2. Furthermore, Franck–Condon factors (FCF) have previously turned out as quite useful in providing additional support for the proposed assignments by simulating the observed vibrational progressions in the photoelectron spectra[25,26] and will therefore be carried out for all relevant ionizations. DFT optimized geometries and harmonic vibrational analyses will be used for these simulations.

COMPUTATIONAL METHODS

All the calculations in this contribution were carried out and are presented by using the C_{2v} point group. Purely for convenience and as can be seen in Figure 1a, the same coordinate system

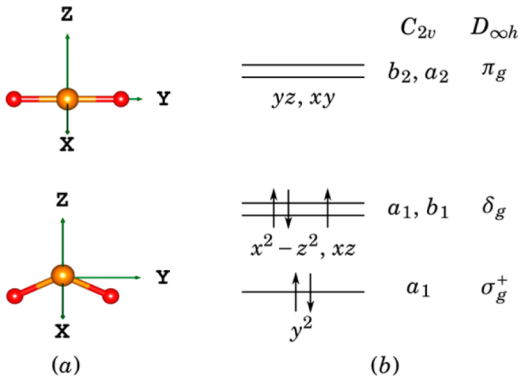

Figure 1. Coordinate system as used in the calculations (a) and qualitative orbital energy scheme for the valence 3d orbitals of iron based on the relative ordering of the low-energy states of FeO_2^- (b). Arrows represent the occupation of its electronic ground state: $^2\Delta_g$.

was employed for the linear and bent geometric structures of the $FeO_2^{-/0}$ clusters. For the bent structure, the three nuclei are placed in the *yz* plane with, as customary, the *z* axis as the 2-fold rotation axis. Consequently, for the linear structure all the nuclei are positioned on the *y* axis. This information about the specific choice of the coordinate system is vital to interpreting the labeling of the molecular orbitals and electronic states. With a few exceptions, nearly all electronic states are predicted to possess a slightly bent structure and very shallow potential energy profiles for the symmetric bending mode. The linear structures are transition states with very small energy barriers. It is therefore allowed and useful to label the C_{2v} states according to the $D_{\infty h}$ parent states from which they originate as a result of Renner–Teller distortions.

Our multireference wave function calculations involve the CASPT2 and RASPT2 methods. At the start of the multireference part of our study, CASPT2 was used to optimize the structures of the low-lying states of $FeO_2^{-/0}$ clusters. Subsequently, single-point RASPT2 calculations were carried out by using the CASPT2 optimized structures. ANO-RCC basis sets with [7s6p4d3f2g] and [5s4p3d2f] contraction schemes were employed for iron and oxygen, respectively.[32,33] Scalar-relativistic effects were included by using the Douglas–Kroll–Hess Hamiltonian.[34,35] To reduce the required memory for storing the two-electron integrals, the Cholesky decomposition with a threshold of 10^{-6} E_h was applied.[36] The CASPT2 and RASPT2 parts of the calculations did not correlate the 1s, 2s, and 2p orbitals of iron and the 1s orbitals of oxygen, while intruder states were treated by applying an imaginary level shift of 0.1. These CASPT2 and RASPT2 calculations were performed with the MOLCAS 7.4 software.[37] The necessary molecular orbitals for CASPT2 and RASPT2 were optimized by complete or restricted active space self-consistent field (CASSCF and RASSCF) calculations, respectively. The active space for the CASSCF calculations included the 2p orbitals of oxygen and the 3d and 4s orbitals of iron, yielding an active space with 16 or 17 electrons distributed among 12 orbitals, which is similar to the one employed in the previous MRCI study.[23] It should be noted that this active space does not cover the double-shell effects of oxygen and iron. In order to do so, the 3p orbitals of oxygen and 3d′ orbitals of iron need to be added to the active space. However, our previous CASPT2 and RASPT2 calculations for the $FeO^{-/0}$ clusters show that the double-shell effect of oxygen atoms is much more important than that of iron,[22,38] and therefore we left out the 3d′ orbitals of iron. An active space with 16 or 17 electrons in 18 orbitals is quite time-consuming and represents an upper limit for what is currently hardware-wise feasible. Fortunately, the RASSCF/RASPT2 represents a sufficient solution for this problem.[39] In the RASSCF step of these calculations, the active space is divided into RAS1, RAS2, and RAS3 subspaces. The 2p orbitals of oxygen and 3d orbitals of iron were included in RAS2, the 3p orbitals of oxygen atoms and the 4s orbital of iron were put in RAS3 with RAS1 left empty. The maximum number of electrons allowed to be excited from RAS2 to RAS3 was SD and SDT (singles, doubles, and triples). This RASSCF active space can be denoted as (16,17;0,*n*;0,11,7) with $n = 2$ (SD) and $n = 3$ (SDT). In summary, during the RASSCF step, the electronic states were expanded in the multielectron basis (symmetry adapted linear combinations of Slater determinants) which comprised all possible distributions of 16 or 17 valence electrons among 11 orbitals of the RAS2 subspace. Additionally, this full expansion was augmented by allowing a maximum number of two (SD) or three (SDT) of these valence electrons to occupy any of the seven orbitals of the RAS3 subspace. In this way, the RASSCF expansion is considerably shorter than the corresponding CASPT2 expansion with the same total amount of active orbitals and electrons as a result of eliminating high energy

configurations. Because of convergence problems, the RASSCF molecular orbitals were only optimized for the SD excitations. The remaining RASSCF calculations (SDT) used these orbitals to perform the corresponding wave function expansions.

All RCCSD(T) calculations were performed with the MOLPRO 2009 software.[40] Restricted open-shell Hartree–Fock (ROHF) wave functions for the electronic configurations were calculated and subsequently used as a reference function for the RCCSD(T) calculations after verifying the correct composition of the open-shell orbitals. Previous extensive experience has shown that coupled cluster methods need large basis sets for obtaining an adequate amount of differential correlation energy between various states of different isomers. In our previous RCCSD(T) study on $FeO_4^{-/0}$ clusters,[26] the aug-cc-pwCVnZ-DK basis sets for iron and aug-cc-pVnZ-DK basis sets for oxygen with n equal to T (triple), Q (quadruple), and 5 (quintuple)[41−43] were used. It was found that the relative energies become stable from the quadruple-ζ basis sets onward. Therefore, in this work, the quadruple-ζ basis sets were used for the manual geometry optimizations of all relevant electronic states. For this purpose, the two Fe–O bonds of the linear structures were first symmetrically stretched. With these intermediate bond distances fixed, the OFeO bond angle was bent. This process was repeated at least twice to ensure that the optimized bond distances and the bond angles are reliable estimates for the minima of the potential energy surfaces. In order to even further improve the calculated ionization energies and relative stabilities, the quintuple-zeta basis sets were used in single-point calculations. Scalar-relativistic effects were again incorporated by using the Douglas–Kroll–Hess Hamiltonian to second-order. All the valence orbitals of oxygen (2s, 2p) and iron (3d, 4s) along with the outer-core orbitals of iron (3s, 3p) were correlated.

With the sole purpose to provide further support for the proposed assignment of the photoelectron spectra, the experimental measured vibrational characteristics were theoretically simulated. Multidimensional Franck–Condon factors were obtained with the MOLFC package.[44] The equilibrium geometries and harmonic vibrational frequencies for these simulations were calculated at the DFT level. All these geometry optimizations and harmonic frequency analyses were performed by applying C_{2v} symmetry and were based on the CASSCF electronic leading configurations. As for iron oxide systems, the pure BP86 functional[45,46] is believed to perform well;[18] this functional was chosen. The def2-QZVP basis sets[47] were used for all atoms, and all DFT calculations were performed with the TURBOMOLE 6.0 suite of programs.[48]

RESULTS AND DISCUSSION

The CASPT2 results in the first part of Table 1 indicate that the $^6A_1$ ($^6\Sigma_g^+$ for the linear structure) state is the lowest state of the anion. The $^2A_1$ and $^2B_1$ states ($^2\Delta_g$) on the one hand and the $^4B_2$ state (a $^4\Pi_g$ component) on the other hand are 0.23 and 0.39 eV higher than the $^6A_1$. For the neutral, the $^3A_1$, $^3B_1$, and $^5B_2$ states have low energies, and therefore one of them might be the true ground state of the neutral. However, it should be noted that the active space for the CASSCF/CASPT2 calculation in this case does not cover the double-shell effects. Therefore, a larger active space should be used for the multireference calculations in order to get more reliable energies. Moreover, it is well-known that in these cases the second-order perturbation theory overestimates the relative stability of the high-spin states as the result of an insufficient recovery of the dynamical correlation energy. In this light, the CASPT2 high-spin $^6A_1$ and $^5B_2$ proposed ground states are suspicious. Thus, the RASPT2 and RCCSD(T) methods need to be applied for these systems as more reliable computational techniques.

Table 1. Adiabatic Relative Energies and Structural Parameters for the Low-Lying States of $FeO_2^{-/0}$ Clusters As Obtained by CASPT2 and RCCSD(T)

method	cluster	state	FeO (Å)	OFeO (deg)	ΔE (eV)
CASPT2	FeO_2^-	$^2A_1$	1.640	180.00	0.00
		$^2B_1$	1.640	180.00	0.00
		$^4A_2$	1.691	176.04	0.34
		$^4B_2$	1.650	130.34	0.16
		$^6A_1$	1.710	151.90	−0.23
	FeO_2	$^3A_1$	1.607	147.33	2.36
		$^3B_1$	1.607	148.94	2.41
		$^5A_2$	1.664	149.47	2.92
		$^5B_2$	1.621	120.88	2.36
		2^3B_1	1.626	140.47	3.29
		$^7A_1$	1.734	174.53	3.87
		$^7A_2$	1.728	124.29	5.49
		$^7B_1$	1.734	169.60	3.87
		$^7B_2$	1.710	122.07	5.38
RCCSD(T)	FeO_2^-	$^2A_1$	1.620	155.42	0.00
		$^2B_1$	1.621	155.01	0.00
		$^4A_2$	1.674	178.09	0.17
		$^4B_2$	1.660	150.23	0.13
		$^6A_1$	1.702	162.64	0.14
	FeO_2	$^3A_1$	1.591	149.39	2.52
		$^3B_1$	1.589	146.42	2.51
		$^5A_2$	1.660	159.71	3.36
		$^5B_2$	1.604	120.92	2.80
		2^3B_1[(a)]	1.642	141.85	3.54

The electronic configurations and the relative energies of the low-lying states of FeO_2 and FeO_2^- as calculated with the RASPT2 method are presented in Table 2. The relative energies become closer when the electron excitations increase from SD to SDT. For the most elaborate SDT calculations, the ground state of the anion is found to be either $^2A_1$ or $^2B_1$, since the energy difference between both doublets is less than 0.01 eV. The $^4A_2$, $^4B_2$, and $^6A_1$ states are also low-lying at less than 0.2 eV above the doublets. For the neutral cluster, the RASPT2 method calculates the $^3A_1$ as its lowest state while the $^3B_1$ and $^5B_2$ are 0.20 and 0.10 eV higher, respectively. Although the splitting between the various low-lying states of FeO_2 and FeO_2^- is small, the low-spin states of the anionic and the neutral clusters are retained as the ground states, reflecting the increased recovery of the nondynamic and dynamic correlation energy. In particular, concerning the identity of the ground state of the anion, our RASPT2 results confirm the conclusion of the previous MRCI study, while the relative positions of the quartet states with respect to the sextet are inverted.[23] Because of the small energy differences, additional support for the so far reached findings are clearly beneficial. In this respect, the $FeO_2^{-/0}$ clusters were further studied at the RCCSD(T) level.

Indeed, from our past experience, RCCSD(T) has been proven itself as an efficient method to predict the ground states for small iron–oxygen clusters.[24,26] In spite of being a single-reference computational method, it has been demonstrated to

Table 2. Electronic Leading Configurations and Relative Energies for the Low-Lying states of $FeO_2^{-/0}$ Clusters As Obtained by RASPT2 and RCCSD(T) Single-Point Calculations

			RASPT2 (eV)			
cluster	state	leading configuration	SD	SDT	RCCSD(T)[a] (eV)	exptl. (eV)
FeO_2^-	$^2A_1$	$9a_1^2 10a_1^1 11a_1^1 3b_1^2 4b_1^2 6b_2^2 7b_2^0 1a_2^2 2a_2^0$	0.00	0.00	0.00	
	2^2A_1[b]	$9a_1^2 10a_1^2 11a_1^1 3b_1^2 4b_1^2 6b_2^2 7b_2^0 1a_2^2 2a_2^0$	0.50	0.52	0.57	
	$^2B_1$	$9a_1^2 10a_1^2 11a_1^2 3b_1^2 4b_1^1 6b_2^2 7b_2^0 1a_2^2 2a_2^0$	0.00	0.00	0.00	
	$^4A_2$	$9a_1^2 10a_1^2 11a_1^1 3b_1^2 4b_1^1 6b_2^2 7b_2^1 1a_2^2 2a_2^0$	0.19	0.14	0.18	
	$^4B_2$	$9a_1^2 10a_1^2 11a_1^1 3b_1^2 4b_1^1 6b_2^2 7b_2^0 1a_2^2 2a_2^1$	0.24	0.13	0.13	
	$^6A_1$	$9a_1^2 10a_1^1 11a_1^1 3b_1^2 4b_1^1 6b_2^2 7b_2^1 1a_2^2 2a_2^1$	0.24	0.18	0.16	
FeO_2	$^3A_1$	$9a_1^2 10a_1^1 11a_1^1 3b_1^2 4b_1^2 6b_2^2 7b_2^0 1a_2^2 2a_2^0$	1.88	1.98	2.53	2.36
	$^3B_1$	$9a_1^2 10a_1^2 11a_1^1 3b_1^2 4b_1^1 6b_2^2 7b_2^0 1a_2^2 2a_2^0$	2.08	2.18	2.52	2.36
	$^5A_2$	$9a_1^2 10a_1^1 11a_1^1 3b_1^2 4b_1^1 6b_2^2 7b_2^1 1a_2^2 2a_2^0$	2.61	2.64	3.39	
	$^5B_2$	$9a_1^2 10a_1^1 11a_1^1 3b_1^2 4b_1^1 6b_2^2 7b_2^0 1a_2^2 2a_2^1$	2.04	2.08	2.82	
	2^3B_1[c]	$9a_1^2 10a_1^1 11a_1^2 3b_1^2 4b_1^1 6b_2^2 7b_2^0 1a_2^2 2a_2^0$	3.00	3.08	3.69	3.31

[a]Aug-cc-pwCV5Z-DK basis sets for iron and aug-cc-pV5Z-DK basis sets for oxygen. [b]Calculated at the geometry of the $^2A_1$ state. [c]Calculated at the geometry of the $^3B_1$ state.

perform very well around the minima of the potential energy surfaces even in those cases that exhibit moderate multireference character. By comparing Tables 1 and 2, it can be deduced that the relative energies of the low-lying states of FeO_2 and FeO_2^- remain almost unchanged when the basis sets are changed from quadruple-ζ to quintuple zeta quality. Even with the former basis sets, the $^2A_1$ and $^2B_1$ states are reconfirmed as the lowest states of the anion, which leaves little doubt that its true ground state has a doublet spin multiplicity. The $^4A_2$, $^4B_2$, and $^6A_1$ states are located 0.18, 0.13, and 0.16 eV higher, respectively. For the neutral cluster, the $^3A_1$ and $^3B_1$ are the lowest states, with the $^5B_2$ distinctively higher at 0.29 eV. So, qualitatively the high-accurate MRCI,[23] RASPT2, and RCSSD(T) results mutually agree on the relative sequence of the various low-lying states, in the sense that they reject the previously proposed quartet and quintet ground states for $FeO_2^{-/0}$. On this basis, the assignment of the anion spectroscopy of the FeO_2 cluster must be re-examined. For this purpose, the potential energy profiles for the two symmetric vibrational C_{2v} modes (stretching and bending) are of importance because only excitations from the totally symmetric vibrational ground state to an excited level of these modes can give substantial Franck–Condon factors for ionizations.

The potential energy curves of the low-lying states of FeO_2 and FeO_2^- as obtained from the RCCSD(T) calculations are shown in Figure 2. With just one exception for the $^5B_2$ state, the profiles for the bending mode of the anionic and neutral low-lying states are very shallow (Figure 2b). This is the reason as to why the calculated bond angles of these clusters are very sensitive to the computational method employed. Further, because of the small splitting of the linear $D_{\infty h}$ states, it is reasonable, and for the sake of clarity beneficial, to use the high-symmetry notation in the following discussion of the electronic structure, even when the symmetry of the actual minima is C_{2v}. For the $^2\Delta_g$ ($^2A_1$, $^2B_1$) states, RCCSD(T) predicts bent structures with an OFeO angle around 155°. In contrast, the CASPT2 method predicts rather surprisingly a linear $^2\Delta_g$ ($^2A_1$, $^2B_1$) state, although it is subject to a Renner–Teller distortion. This result agrees very well with the previous MRCI theoretical study and infrared spectroscopical results.[23] However, most certainly, the small extent of the Renner–Teller effect is at the origin of these observations and therefore does not constitute a serious discrepancy. Indeed, the energy barrier for the inversion of the OFeO bond angle is as small as 116 cm^{-1} at the RCCSD(T) level, meaning that at room temperature the anionic cluster is vibrating between the two minima, explaining

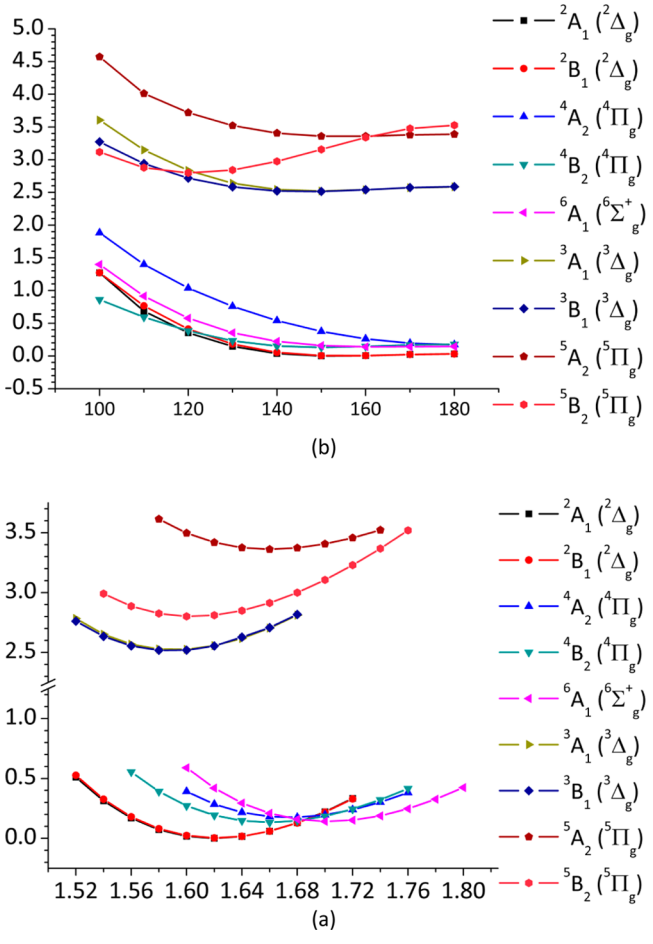

Figure 2. Potential energy curves for the low-lying states of $FeO_2^{-/0}$ calculated at the RCCSD(T) level (quadruple-ζ basis sets): (a) stretching mode (bond angle fixed at its equilibrium value of Table 1) and (b) bending mode (bond distance fixed at its equilibrium value of Table 1). Abscissa: (a) Fe–O bond distance in Å, (b) O–Fe–O bond angle in degrees. Ordinate: energies in eV.

dx.doi.org/10.1021/ct300516y | J. Chem. Theory Comput. 2012, 8, 3089–3096

that infrared spectrometry suggests a linear ground state for the anion.[23] For $^3A_1$ and $^3B_1$, both methods employed in this work calculate a bent structure with an OFeO angle that is somewhat smaller than 150°. Also, these methods agree that $^5B_2$ has, of all states considered, with a bond angle of around 120° the most pronounced bent equilibrium structure (see Table 1). Since, the experimental angle is estimated to be in the range from 144° to 158°,[8] it must be concluded that the ground state of the neutral cluster is a triplet, which indirectly renders additional credibility for the $^2\Delta_g$ ground state for the anion as proposed in the preceding paragraph on the basis of the RASPT2 and RCCSD(T) energies.

The photoelectron spectra of FeO_2^- were measured with 3.49 and 4.66 eV detachment photon energies, with the latter one depicted in Figure 3.[12−14] In these spectra, only two bands

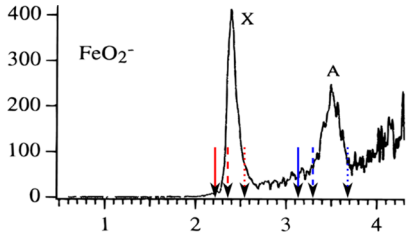

Figure 3. Experimental photoelectron spectrum of FeO_2- taken from ref 13. Abscissa: binding energies in eV. Ordinate: relative detached electron intensities. The dashed, full line and dotted arrows represent the adiabatic detachment energies as calculated by CASPT2, RASPT2, and RCCSD(T), respectively.

at 2.36 and 3.31 eV were observed. Both are relatively broad bands with no clear vibrational progression. This implies that the equilibrium geometries of the initial and final state for the two ionization processes are very similar, indicating that electrons are detached from nonbonding molecular orbitals. The broadness of these bands is believed to originate from the low frequency bending mode of FeO_2. The estimated instrumental resolution suggests that this frequency is smaller than 350 cm^{-1} for the X band.[12] A slightly more pronounced vibrational progression of the A band in the 4.66 eV spectrum indicates that the frequency of the bending mode of the underlying final state is somewhat larger than that of the X band.[13]

Our proposed assignment is based on the calculated relative energies of Table 2 and the application of the one-electron detachment selection rule. From the electronic configurations of the low-lying states of $FeO_2^{-/0}$ also given in Table 2, it can be deduced that there are several one-electron ionizations with adiabatic detachment energies (ADEs) around 3 eV which can possibly correspond to one of the two bands of the spectrum. They are the $^2\Delta_g(^2A_1, {}^2B_1)\rightarrow{}^3\Delta_g(^3A_1, {}^3B_1)$, $^4\Pi_g(^4A_2, {}^4B_2)\rightarrow{}^3\Delta_g(^3A_1, {}^3B_1)$, and $^6\Sigma_g^+(^6A_1)\rightarrow{}^5\Pi_g$ ($^5A_2$, $^5B_2$) ionizations. Nevertheless, the quartet and sextet states are higher in energy at the highest levels of computation, cf. the RASPT2 and RCCSD(T) results of Table 2; multidimensional Franck−Condon factors were calculated for the lowest single electron detachment processes from these states with the purpose to compare them with the shape of experimental bands. The Franck−Condon factors which were obtained by using the BP86 frequencies are depicted in Figure 4. We first examine the possible ionizations for the X band. The $^4A_2\rightarrow{}^3A_1$ (Figure 4a) and $^6A_1\rightarrow{}^5B_2$ (Figure 4e) ionizations which have suitable ADEs of 2.35 and 2.66 eV at the RCCSD(T) level would result in broad vibrational progressions due to excitations in the symmetric stretching modes of 908 cm^{-1} and 907 cm^{-1} of the $^3A_1$ and $^5B_2$ states. Indeed, the obtained progressions are the result of the removal of an electron from an antibonding d_π orbital, causing the Fe−O bond distance to shorten from 1.676 Å to 1.587 Å for the $^4A_2\rightarrow{}^3A_1$ ionization and from 1.708 Å to 1.611 Å for $^6A_1\rightarrow{}^5B_2$. As the bond angle changes by 20° and 40°, bending mode transitions with frequencies ranging from 200 cm^{-1} to 300 cm^{-1} (see Table 1) are superimposed on these symmetric stretching transitions. Combined they result in extremely broad structureless bands with band widths of at least 0.6 eV, which is about twice the experimental bandwidth of 0.3 eV for the X band in Figure 3. According to Figure 4b, the $^4B_2\rightarrow{}^3B_1$ transition, which on the basis of the RCCSD(T) results of Table 2 would occur at 2.39 eV, should be observed as a progression with an interspacing between the constituent peaks of 918 cm^{-1}. This reflects the shortening of the FeO bonds from 1.637 Å to 1.584 Å, while the OFeO angle increases by less than 10°. The measured X band in Figure 3 definitely does not show such a silhouette. For the A band, the $^4A_2\rightarrow{}^5A_2$ ionization with a RCCSD(T) ADE of 3.21 eV could be responsible. However, the corresponding Franck−Condon factors in Figure 4c would afford a very pronounced broad band of around 1 eV, which is considerably larger than the experimental bandwidth of 0.4 eV in Figure 3. The remaining two ionizations from the quartet and sextet states, i.e., $^4B_2\rightarrow{}^5B_2$ and $^6A_1\rightarrow{}^5A_2$ in Figure 4d and f, which would give rise to narrow bands, are to be eliminated because the associated lower energy ionizations $^4B_2\rightarrow{}^3B_1$ and $^6A_1\rightarrow{}^5B_2$ should also be observed in the experimental spectrum but were already rejected. As a final conclusion, the calculated detachment energies and Franck−Condon factors allow one to definitely rule out the quartet and sextet states as being the initial states responsible for the observed photoelectron spectroscopy of FeO_2^-.

On the other hand, the Franck−Condon factors for the $^2\Delta_g\rightarrow{}^3\Delta_g$ ionizations in Figure 5 show vibrational progressions of just two peaks with a frequency of 908 cm^{-1} for the $^2A_1\rightarrow{}^3A_1$ component (Figure 5a) of this ionization. The intensity of the transition to the second level of the symmetric stretching mode of the neutral cluster state is considerably less. Additionally, the $^2B_1\rightarrow{}^3B_1$ component in Figure 5b has a progression originating from the bending mode with a frequency of 203 cm^{-1}. However, this interspacing is definitely smaller than the resolution of the photoelectron spectrum and is therefore not observed. This effect will broaden the symmetric stretching mode peaks for the $^2B_1\rightarrow{}^3B_1$ ionization, which when combined with a small displacement for the $^2A_1\rightarrow{}^3A_1$ component will lead to a relatively broad band with a shoulder at the high-energy end. When compared with the shape of the X band in Figure 3, we can reach the conclusion that this is indeed a good match. Both transitions involve the removal of an electron from the mainly nonbonding to slightly antibonding d_σ orbital, which explains the small changes for the Fe−O bond length from 1.610 Å for $^2A_1$ and 1.618 Å for $^2B_1$ to 1.587 Å for $^3A_1$ and 1.584 Å for $^3B_1$, and the resulting very limited extent of the vibrational progression. The corresponding adiabatic detachment energies are calculated at 1.98 and 2.18 eV by RASPT2, while RCCSD(T) predicts larger but less different values of 2.53 and 2.52 eV. Experimentally, the X band starts at a value of 2.36 eV, which is in the middle of the RASPT2 and RCCSD(T)

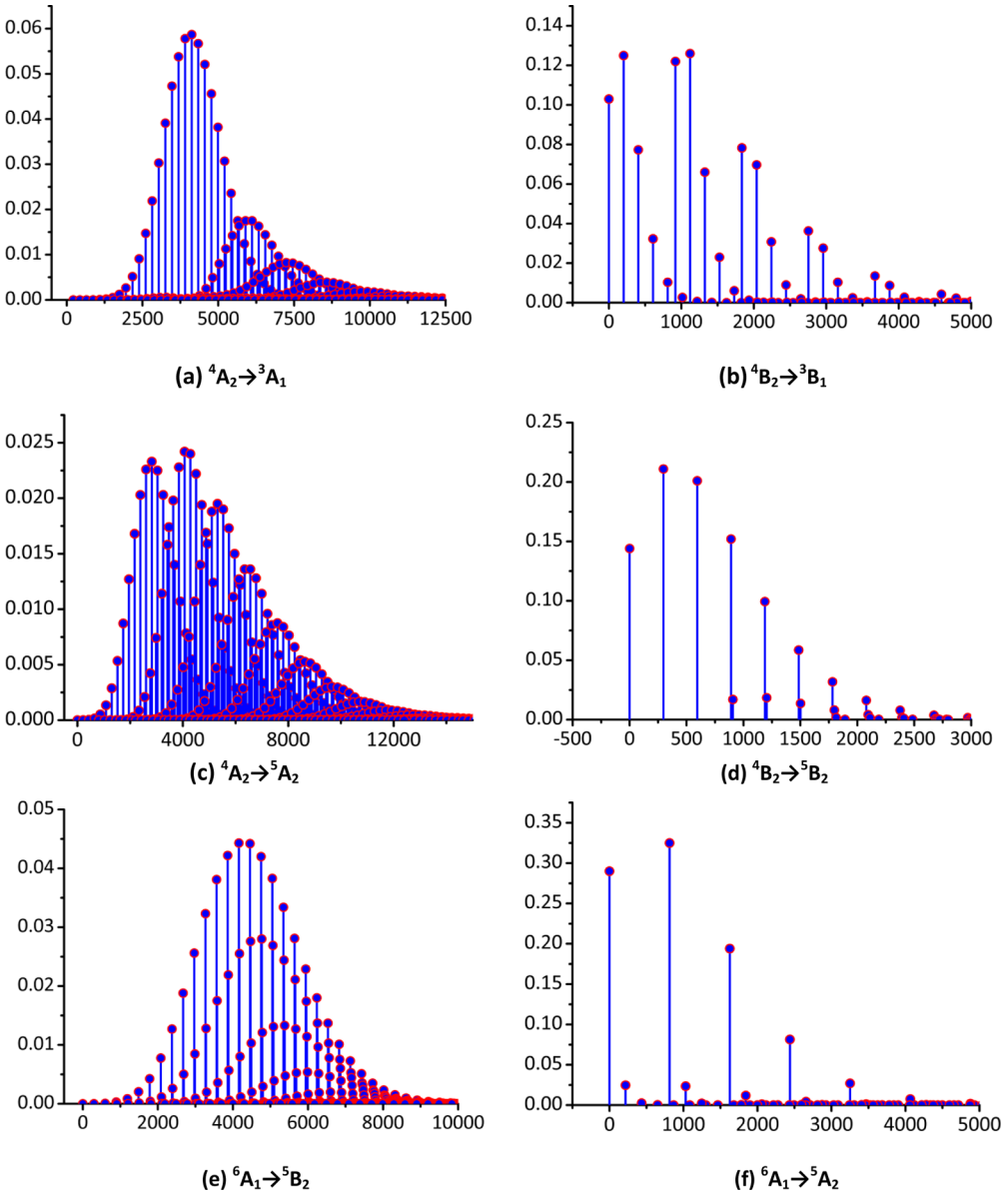

Figure 4. Franck−Condon factors for the (a) $^4A_2 \rightarrow {}^3A_1$, (b) $^4B_2 \rightarrow {}^3B_1$, (c) $^4A_2 \rightarrow {}^5A_2$, (d) $^4B_2 \rightarrow {}^5B_2$, (e) $^6A_1 \rightarrow {}^5B_2$, and (f) $^6A_1 \rightarrow {}^5A_2$ ionizations based on the BP86 optimized C_{2v} bent structures and harmonic frequencies. The calculated shapes of these vibrational progressions allow one to reject these ionizations as being responsible for the experimental photoelectron spectrum. Abscissa: frequencies of the vibrational progressions in cm^{-1}. Ordinate: relative intensities.

results. Therefore, both the Franck−Condon factors and the calculated adiabatic detachment energies univocally assign the X band of the photoelectron spectrum of FeO_2^- to the $^2\Delta_g \rightarrow {}^3\Delta_g$ transition. Also, the A band of the photoelectron spectrum can be accounted for as an ionization from the $^2\Delta_g$ anionic ground state. In this case, the final state is $^3\Sigma_g^+$ (2^3B_1) as the result of an electron detachment from the nonbonding d_δ orbitals, i.e., orbitals $10a_1$ and $4b_1$. As can be deduced from Table 1, the bond lengths increase hardly by less than 0.02 Å at the CASPT2 and RCCSD(T) levels. Consequently, no vibrational progression is expected for these ionizations. However, this could not be verified at the BP98 level because the 2^3B_1 ($^3\Sigma_g^+$) state has an electronic configuration which only differs from the lower-lying 1^2B_1 in the occupation of the $10a_1$ and $11a_1$ orbitals. As an alternative, a vibrational analysis for the linear $^2\Delta_g \rightarrow {}^3\Sigma_g^+$ ionization at the RCCSD(T) level yielded no progression whatsoever, as depicted in Figure 5d. The adiabatic detachment energies for this ionization are evaluated to be 3.08 and 3.69 eV by the RASPT2 and RCCSD(T) methods, respectively. Again the experimentally proposed value of 3.31 eV is intermediate to these two these values.

CONCLUSION

All low-lying states of the $FeO_2^{-/0}$ clusters have a bent C_{2v} geometry as the global minimum. The RCCSD(T) potential energy profiles of the bending vibrational mode for the spectroscopic relevant states are however extremely shallow with small energy barriers for the bond angle inversion as a result. Also, the calculated splittings of the various low-lying linear states are negligibly small. Both observations allow a more simple analysis of the electronic structures in terms of the $D_{\infty h}$ point group. The small energy difference between the low-lying states is the reason why the identification of the ground states for the neutral and anionic clusters is exceptionally

dx.doi.org/10.1021/ct300516y | J. Chem. Theory Comput. 2012, 8, 3089−3096

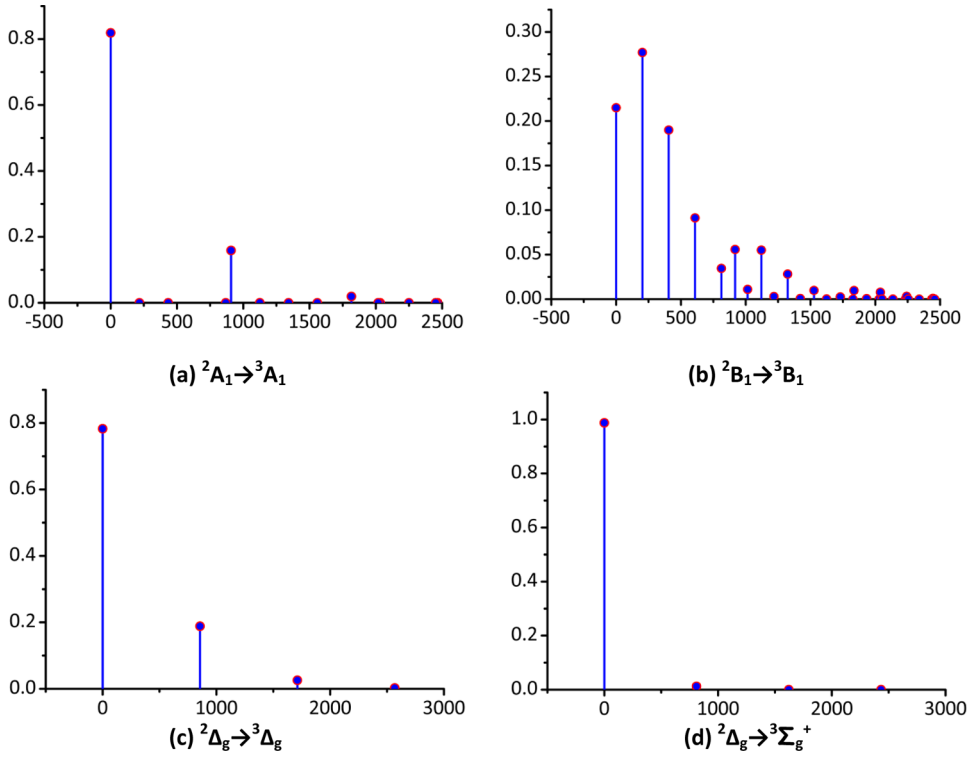

Figure 5. Franck–Condon factors for the $^2A_1 \rightarrow ^3A_1$ (a) and the $^2B_1 \rightarrow ^3B_1$ (b) ionization based on the BP86 optimized bent C_{2v} structures and harmonic frequencies and Franck–Condon factors for the symmetric stretching vibrational mode as calculated from the RCCSD(T) potential energy curves for the (c) $^2\Delta_g \rightarrow ^3\Delta_g$ and (d) $^2\Delta_g \rightarrow ^3\Sigma_g^+$ ionizations. Parts a and b combined and c individually represent a simulation for experimental X band. Part d corresponds to the A band. Abscissa: frequencies in cm^{-1}. Ordinate: relative intensities.

difficult. Depending on the method used, a triplet or quintet is obtained as the lowest electronic state for the former cluster, while the ground state for the latter is calculated to possess either a doublet, quartet, or sextet spin multiplicity. Only for the most elaborate RASPT2 and RCCSD(T) calculations does the $^2\Delta_g$ appear as the anionic ground state, whereas for the neutral, the $^3\Delta_g$ state has the highest stability. Therefore, the single-reference RCCSD(T) appears appropriate to describe these very difficult-to-calculate species. Under the influence of the linear ligand field interactions and the 3d–4s mixing, the iron cation d orbitals split into three levels: two essential nonbonding levels made up of the d_σ or d_δ orbitals and an antibonding d_π level. The X band of the photoelectron spectrum originates from the $^2\Delta_g \rightarrow ^3\Delta_g$ transition. The A band is assigned to the $^2\Delta_g \rightarrow ^3\Sigma_g^+$ ionization. This assignment of the anion photoelectron spectrum is confirmed by Franck–Condon factors as obtained from the BP86 optimized structures and harmonic vibrational frequencies. The absence of a clear vibrational progression in the experimental spectrum is therefore ascribed to ionization from the nonbonding d_σ orbital for the X band and from the ditto d_δ level for the A band. The broadness of both bands is the result of transitions to excited levels of the symmetric bending mode.

AUTHOR INFORMATION

Corresponding Author

*E-mail: marc.hendrickx@chem.kuleuven.be.

Notes

The authors declare no competing financial interest.

REFERENCES

(1) Chen, H.; Ikeda-Saito, M.; Shaik, S. *J. Am. Chem. Soc.* **2008**, *130*, 14778.
(2) Xue, W.; Wang, Z. C.; He, S. G.; Xie, Y.; Bernstein, E. R. *J. Am. Chem. Soc.* **2008**, *130*, 15879.
(3) Momenteau, M.; Reed, C. A. *Chem. Rev. (Washington, DC, U. S.)* **1994**, *94*, 659.
(4) Kovaleva, E. G.; Neibergall, M. B.; Chakrabarty, S.; Lipscomb, J. D. *Acc. Chem. Res.* **2007**, *40*, 475.
(5) Lu, Z. H.; Xu, Q. *J. Chem. Phys.* **2011**, *134*, 034305.
(6) Gong, Y.; Zhou, M. F.; Andrews, L. *Chem. Rev. (Washington, DC, U. S.)* **2009**, *109*, 6765.
(7) Yamada, Y.; Sumino, H.; Okamura, Y.; Shimasaki, H.; Tominaga, T. *Appl. Radiat. Isot.* **2000**, *52*, 157.
(8) Chertihin, G. V.; Saffel, W.; Yustein, J. T.; Andrews, L.; Neurock, M.; Ricca, A.; Bauschlicher, C. W. *J. Phys. Chem.* **1996**, *100*, 5261.
(9) Gong, Y.; Zhou, M. F.; Andrews, L. *J. Phys. Chem. A* **2007**, *111*, 12001.
(10) Andrews, L.; Chertihin, G. V.; Citra, A.; Neurock, M. *J. Phys. Chem.* **1996**, *100*, 11235.
(11) Andrews, L.; Chertihin, G. V.; Ricca, A.; Bauschlicher, C. W. *J. Am. Chem. Soc.* **1996**, *118*, 467.
(12) Fan, J. W.; Wang, L. S. *J. Chem. Phys.* **1995**, *102*, 8714.
(13) Wu, H. B.; Desai, S. R.; Wang, L. S. *J. Am. Chem. Soc.* **1996**, *118*, 7434.
(14) Wu, H. B.; Desai, S. R.; Wang, L. S. *J. Am. Chem. Soc.* **1996**, *118*, 5296.
(15) Wang, L. S.; Wu, H. B.; Desai, S. R. *Phys. Rev. Lett.* **1996**, *76*, 4853.
(16) Cao, Z. X.; Duran, M.; Sola, M. *Chem. Phys. Lett.* **1997**, *274*, 411.
(17) Garcia-Sosa, A. T.; Castro, M. *Int. J. Quantum Chem.* **2000**, *80*, 307.
(18) Gutsev, G. L.; Khanna, S. N.; Rao, B. K.; Jena, P. *J. Phys. Chem. A* **1999**, *103*, 5812.
(19) Gong, Y.; Zhou, M. F. *J. Phys. Chem. A* **2008**, *112*, 10838.

(20) Atanasov, M. *Inorg. Chem.* **1999**, *38*, 4942.
(21) Gutsev, G. L.; Weatherford, C. A.; Pradhan, K.; Jena, P. *J. Phys. Chem. A* **2010**, *114*, 9014.
(22) Hendrickx, M. F. A.; Anam, K. R. *J. Phys. Chem. A* **2009**, *113*, 8746.
(23) Li, Z. H.; Gong, Y.; Fan, K. N.; Zhou, M. F. *J. Phys. Chem. A* **2008**, *112*, 13641.
(24) Sakellaris, C. N.; Miliordos, E.; Mavridis, A. *J. Chem. Phys.* **2011**, *134*, 234308.
(25) Tran, V. T.; Hendrickx, M. F. A. *J. Chem. Theory Comput.* **2011**, *7*, 310.
(26) Tran, V. T.; Hendrickx, M. F. A. *J. Chem. Phys.* **2011**, *135*, 094505.
(27) Tran, V. T.; Hendrickx, M. F. A. *J. Phys. Chem. A* **2011**, *115*, 13956.
(28) Gutsev, G. L.; Rao, B. K.; Jena, P. *J. Phys. Chem. A* **2000**, *104*, 11961.
(29) Uzunova, E. L.; St. Nikolov, G.; Mikosch, H. *ChemPhysChem* **2004**, *5*, 192.
(30) Uzunova, E. L.; Mikosch, H.; Nikolov, G. S. *J. Chem. Phys.* **2008**, *128*, 094307.
(31) Grein, F. *Int. J. Quantum Chem.* **2009**, *109*, 549.
(32) Roos, B. O.; Lindh, R.; Malmqvist, P. A.; Veryazov, V.; Widmark, P. O. *J. Phys. Chem. A* **2005**, *109*, 6575.
(33) Roos, B. O.; Lindh, R.; Malmqvist, P. A.; Veryazov, V.; Widmark, P. O. *J. Phys. Chem. A* **2004**, *108*, 2851.
(34) Hess, B. A. *Phys. Rev. A* **1986**, *33*, 3742.
(35) Douglas, M.; Kroll, N. M. *Ann. Phys* **1974**, *82*, 89.
(36) Aquilante, F.; Pedersen, T. B.; Lindh, R.; Roos, B. O.; De Meras, A. S.; Koch, H. *J. Chem. Phys.* **2008**, *129*, 8.
(37) Aquilante, F.; De Vico, L.; Ferre, N.; Ghigo, G.; Malmqvist, P. A.; Neogrady, P.; Pedersen, T. B.; Pitonak, M.; Reiher, M.; Roos, B. O.; Serrano-Andres, L.; Urban, M.; Veryazov, V.; Lindh, R. *J. Comput. Chem.* **2010**, *31*, 224.
(38) Vancoillie, S.; Zhao, H.; Tran, V. T.; Hendrickx, M. F. A.; Pierloot, K. *J. Chem. Theory Comput.* **2011**, *7*, 3961.
(39) Gagliardi, L.; Sauri, V.; Serrano-Andres, L.; Shahi, A. R. M.; Vancoillie, S.; Pierloot, K. *J. Chem. Theory Comput.* **2011**, *7*, 153.
(40) Werner, H.-J.; Knowles, P. J.; Knizia, G.; Manby, F. R.; Schütz, M. et al. MOLPRO, version 2010.1; see http://www.molpro.net (accessed August 2012).
(41) Balabanov, N. B.; Peterson, K. A. *J. Chem. Phys.* **2005**, *123*, 15.
(42) Dunning, T. H. *J. Chem. Phys.* **1989**, *90*, 1007.
(43) Kendall, R. A.; Dunning, T. H.; Harrison, R. J. *J. Chem. Phys.* **1992**, *96*, 6796.
(44) Borrelli, R.; Peluso, A. *J. Chem. Phys.* **2006**, *125*, 194308.
(45) Becke, A. D. *Phys. Rev. A* **1988**, *38*, 3098.
(46) Perdew, J. P. *Phys. Rev. B* **1986**, *33*, 8822.
(47) Ahlrichs, R.; Weigend, F.; Furche, F. *J. Chem. Phys.* **2003**, *119*, 12753.
(48) Ahlrichs, R.; Bar, M.; Haser, M.; Horn, H.; Kolmel, C. *Chem. Phys. Lett.* **1989**, *162*, 165.